Conductance of quantum point contacts in the presence of disorder

Y. Takagaki and D. K. Ferry

Center for Solid State Electronics Research, Arizona State University, Tempe, Arizona 85287-6206

We have calculated the conductance of a two-dimensional electron gas through single and double constrictions using a mode-matching technique. In order to take into account the smooth variation of the confinement potential, and the presence of disorder, the calculation is made within a lattice model. We find that the conductance at plateaus is reduced below the quantized values if short-range scatterers are introduced in the channel. However, the conductance remains well quantized even in the presence of long-range impurities. These observations explain the suppression of conductance time-dependent fluctuations at plateaus experimentally observed by Timp *et al.* [Phys. Rev. B **42**, 9259 (1990)]. We also examine the effects of impurities on the resonant transmission properties through a single quantum dot. As the disorder is introduced, the resonances are broadened in energy and can appear as either peaks or dips depending on the strength of the disorder.

I. INTRODUCTION

Recent advances in microfabrication technology have made it possible to realize quantum ballistic electron transport in a two-dimensional electron gas (2DEG) in GaAs-Al$_x$Ga$_{1-x}$As heterostructures. A split-gate technique has been developed by Thornton *et al.*[1] to achieve one-dimensional (1D) systems with controllable width. By applying negative bias to two metal gates, fabricated by lift-off on top of the heterostructure, a narrow channel is left between the pinched-off regions. The conductance of the narrow channel has been found to be quantized in steps of $2e^2/h$, as the number of 1D subbands in the channel is varied as a function of the applied gate voltage.[2] A variety of theoretical studies have been presented, using various techniques to investigate the accuracy of the quantization, and the quantization can be understood easily if the narrow constriction is widened into 2DEG leads adiabatically.[3] The absence of intermode scattering is not, however, a necessary condition for the quantization. In the opposite limit of abrupt geometry, where strong mixing occurs between 1D modes as the electron passes through the wide-narrow junction, the conductance has also been found to be quantized.[4,5] It has been pointed out that an oscillation due to multiple reflections between the exits of the constriction is superposed on the conductance plateaus in the abrupt geometry. The actual geometry in real devices is thought to lie between these two limits, since the oscillation is not observed under usual experimental conditions. Therefore, one needs to include the flared geometry at the exits of the channel in any realistic simulation.

The most important criterion for the conductance quantization phenomena is that the sample length must be less than the elastic mean free path. The effect of scattering from random impurities has been investigated with the assumption of a δ-function potential.[6-9] However, experimental observations suggest that a long-ranged potential in GaAs plays an essential role in the deterioration of the plateaus.[10,11] The quantization breaks down even when the sample length is an order of magnitude less than the transport mean free path l_e.[10] Because of the preferential forward scattering in GaAs, l_e (estimated from the mobility) appears much larger than the mean distance between total elastic-scattering events.[12] Recently, Timp and co-workers[11] observed time-dependent fluctuations of the conductance with an amplitude of $\sim e^2/h$ in a point contact. A population fluctuation at an impurity state causes bilevel switching phenomena of the conductance in small devices.[13] The trapping and detrapping of an electron in the localized state change the local potential, and give rise to a random telegraph signal in the current. It has been observed that the fluctuations are completely inhibited at the center of the plateaus.[11]

A simple mode-matching technique is one of the simplest ways to characterize electron waveguide structures.[5,14] However, the application is limited to some special geometries, and an abrupt connection between the narrow constriction and wide regions is usually assumed. The smooth potential variation and the presence of impurities in real devices have been usually incorporated using the lattice Green's-function technique.[15] In this paper, we extend the mode-matching technique to a lattice model in order to take into account the arbitrary confinement potential and the presence of disorder in the channel. The calculation of the transmission coefficients is based on the transfer-matrix technique. Numerical calculations are performed on single and double point-contact geometries. It will be demonstrated that the change in the conductance at the plateaus due to the presence of disorder is suppressed when the long-range nature of the impurity potential is taken into account.

II. NUMERICAL APPROACH

A. Confinement potential

Let us consider a wire with length L and width W, in which arbitrary model potentials are introduced. A self-consistent calculation of an electrostatic potential in the split-gate geometry[16] has indicated that the confinement potential is almost parabolic when only a few modes are occupied below the Fermi energy. As the channel is widened, the confinement potential possesses a flat bottom between parabolic walls. Therefore, we will assume the following confinement potential in the wire:

$$V(x,y) = V_B(x) + E_F \left[\frac{|y| - y_0(x)}{d} \right]^2$$

$$\times \theta[|y| - y_0(x)] + V_{\mathrm{HW}}(y) , \qquad (1)$$

where $\theta(t)$ is a step function, defined by $\theta = 0$ for $t < 0$ and $\theta = 1$ for $t > 0$, and $V_{\mathrm{HW}}(y)$ is a hard-wall potential defined by $V_{\mathrm{HW}} = 0$ for $|y| < W/2$ and $V_{\mathrm{HW}} = \infty$ for $|y| > W/2$. We assume that $y_0(y)$, which determines the boundary between the parabolic wall and the flat bottom, is given by

$$y_0(x) = \begin{cases} \dfrac{W}{4} \left[\dfrac{4|x|}{L} \right]^p, & |x| < \dfrac{L}{4} \\[3mm] \dfrac{W}{2} \left[1 - \dfrac{1}{2} \left[2 - \dfrac{4|x|}{L} \right]^p \right], & \dfrac{L}{4} < |x| < \dfrac{L}{2} . \end{cases} \qquad (2)$$

The parameter p characterizes the abruptness of the constriction as shown in the upper half of Fig. 1. At $x = 0$ the confinement potential is parabolic. The width of the constriction is determined by the parameter d and throughout this paper we assume $d = \lambda_F$. The propagation threshold for the nth mode, at the narrowest part, is given by

$$\frac{E_n - U}{E_F} = \frac{\lambda_F}{\pi d} (n - \tfrac{1}{2}) . \qquad (3)$$

In the vicinity of the constriction the potential is raised above the conduction-band edge in the 2DEG region due to a proximity effect, and so we assume the bottom potential $V_B(x)$ to be

$$V_B(x) = \begin{cases} U \left[1 - \dfrac{1}{2} \left[\dfrac{4|x|}{L} \right]^p \right], & |x| < \dfrac{L}{4} \\[3mm] \dfrac{U}{2} \left[2 - \dfrac{4|x|}{L} \right]^p, & \dfrac{L}{4} < |x| < \dfrac{L}{2} . \end{cases} \qquad (4)$$

The lower half of Fig. 1 shows an example of the potential profile at the Fermi energy for $U/E_F = 0$, 0.5, and 1. The potential in the two perfect lead regions attached to each end of the wire $(|x| > L/2)$ is solely given by $V(x,y) = V_{\mathrm{HW}}(y)$.

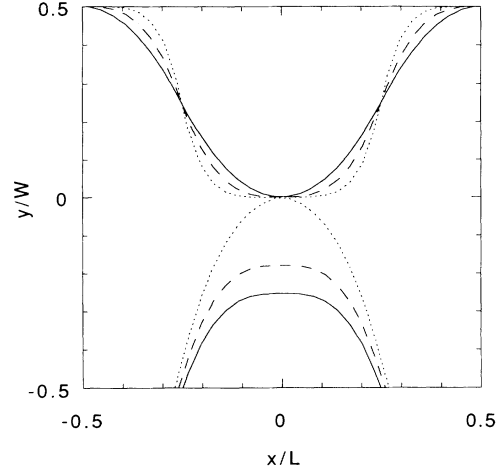In order to apply the mode-matching technique to the smooth potential variation, we divide the system into N_x

FIG. 1. A schematic illustration of a quantum point contact. The upper half shows $y_0(x)$, which is the position of the boundary between parabolic walls and a flat bottom. The solid, dashed, and dotted lines correspond to $p = 2$, 3, and 5, respectively. A potential profile at Fermi energy is shown in the lower half for $p = 3$. The solid, dashed, and dotted lines correspond to the height of the bottom potential $U/E_F = 0$, 0.05, and 1, respectively.

consecutive segments, with lattice constant a $(L = N_x a)$ along the wire. The potential is assumed to be independent of x in each segment. The Schrödinger equation in the segment j $[-L/2 + (j-1)a < x < -L/2 + ja]$ is thus given, within the effective-mass approximation, by

$$\left[-\frac{\hbar^2}{2m} \left[\frac{\partial^2}{\partial x^2} + \frac{\partial^2}{\partial y^2} \right] + V^{(j)}(y) + V_{\mathrm{HW}}(y) \right] \Psi^{(j)}(x,y)$$

$$= E_F \Psi^{(j)}(x,y) . \qquad (5)$$

The general solution of the wave function is expressed in terms of a superposition of the eigenmodes $\chi_n^{(j)}(y)$ in the y direction:

$$\Psi^{(j)}(x,y) = \sum_n (A_n^{(j)} \exp[iq_n^{(j)}x] + B_n^{(j)} \exp[-iq_n^{(j)}x]) \chi_n^{(j)}(y) , \qquad (6)$$

where $\chi_n^{(j)}(y)$ satisfy the 1D Schrödinger equation

$$\left[-\frac{\hbar^2}{2m} \frac{d^2}{dy^2} + V^{(j)}(y) + V_{\mathrm{HW}}(y) \right] \chi_n^{(j)}(y) = E_n^{(j)} \chi_n^{(j)}(y) . \qquad (7)$$

The subband thresholds $E_n^{(j)}$ are related to $q_n^{(j)}$ as

$$q_n^{(j)} = \frac{\sqrt{2m(E_F - E_n^{(j)})}}{\hbar} . \qquad (8)$$

In the two semi-infinite strips, the eigenfunctions have the form

$$\chi_n(y) \equiv u_n(y) = \left[\frac{2}{W} \right]^{1/2} \sin \left[\frac{n\pi}{W} \left[y + \frac{W}{2} \right] \right] . \tag{9}$$

The eigenfunctions in the uniform waveguide section in the presence of the point-contact potential can be expanded in terms of $u_n(y)$:

$$\chi_n^{(j)}(y) = \sum_l f_{nl}^{(j)} u_l(y) . \tag{10}$$

The expansion coefficients $f_{nl}^{(j)}$ are given as a solution of the following eigenvalue equations:

$$\sum_i (l^2 \delta_{il} + K_{li}^{(j)}) f_{ni}^{(j)} = \frac{2mW^2}{\pi^2 \hbar^2} E_n^{(j)} f_{nl}^{(j)} , \tag{11}$$

where

$$K_{li}^{(j)} = \frac{2mW^2}{\pi^2 \hbar^2} \int u_l(y) V^{(j)}(y) u_i(y) dy . \tag{12}$$

The eigenfunctions are normalized and thus satisfy the orthogonality relation

$$\sum_l f_{il}^{(j)} f_{jl}^{(j)} = \delta_{ij} . \tag{13}$$

We again divide each segment into N_y grids with lattice constant a ($W = N_y a$) so as to integrate Eq. (12) numerically for arbitrary potentials. We thus have N_y right- and left-going states in each segment. One can introduce the scattering from short-range impurities through randomness of the site energy, distributed uniformly between $-\Gamma/2$ and $\Gamma/2$. It is useful to express the randomness in terms of the mean free path Λ. In a 2D system, we have

$$\Lambda = \frac{6\lambda_F^3}{\pi^3 a^2} \left[\frac{E_F}{\Gamma} \right]^2 . \tag{14}$$

B. Transfer-matrix technique

Transmission coefficients through the entire lattice are evaluated using the transfer-matrix technique. Imposing the boundary conditions between jth and $(j+1)$th segments at $x = ja$, one obtains the relation

$$\begin{bmatrix} A^{(j+1)} \\ B^{(j+1)} \end{bmatrix} = T^{(j)} \begin{bmatrix} A^{(j)} \\ B^{(j)} \end{bmatrix} = \begin{bmatrix} T_{11}^{(j)} T_{12}^{(j)} \\ T_{21}^{(j)} T_{22}^{(j)} \end{bmatrix} \begin{bmatrix} A^{(j)} \\ B^{(j)} \end{bmatrix} , \tag{15}$$

where $A^{(j)}$ and $B^{(j)}$ are vectors describing the amplitude of the modes in the jth segment and $T_{ij}^{(j)}$ are $N_y \times N_y$ matrices. The transfer matrix for the entire system is given as

$$T = T^{(N_x)} T^{(N_x - 1)} \cdots T^{(0)} . \tag{16}$$

When an electron is incident through mode n in the left-hand lead, the wave function in the right-hand lead is given as a superposition of all right-moving waves:

$$\Psi_n(x,y) = \sum_m t_{mn} e^{ik_m x} u_m(y) , \tag{17}$$

where

$$k_m = \left[\frac{2mE_F}{\hbar^2} - \left[\frac{m\pi}{W} \right]^2 \right]^{1/2} . \tag{18}$$

and t_{mn} are the transmission coefficient from mode n in the left-hand lead to mode m in the right-hand lead. One can obtain the wave function in the left-hand lead using (16) and (17), and hence we have the following set of equations:

$$\sum_m t_{mn} (T^{-1})_{lm} = \delta_{nl} , \tag{19a}$$

$$\sum_m t_{mn} (T^{-1})_{l + N_y m} = r_{nl} , \tag{19b}$$

where r_{nl} are the reflection coefficient from mode l to mode n in the left-hand lead. Therefore, one can evaluate the transmission probabilities $T_{mn} = (k_m / k_n) |t_{mn}|^2$ which are related to the conductance of the system through the Landauer formula[17]

$$G = \frac{2e^2}{h} \sum_{m,n} T_{mn} , \tag{20}$$

where the sum runs over the propagating modes. The numerical stability is monitored through the unitarity $\sum_m (T_{mn} + R_{mn}) = 1$. Here, $R_{mn} = (k_m / k_n) |r_{mn}|^2$ are the reflection probabilities.

III. RESULTS AND DISCUSSION

In this section we present numerical results for the point-contact and quantum-dot structures. The lattice system simulates a continuum system if $a \ll \lambda_F$. Therefore, we consider $N_x = N_y = 32$ lattice sites and assume that $\lambda_F / a = 8.1$.

A. Single point contact

Let us first consider the case of no impurities. Figure 2 shows the conductance of the single point contact as a function of the potential height U at the saddle for $p = 2$, 3, and 5. For $p = 2$ the effective length of the point contact is small, and so the quantization is not well developed.[5,18] With increasing p, the length of the constriction is increased and the transition region for the flared horn becomes short compared to the constriction length. Therefore, the conductance becomes well quantized and then goes below the quantized values because of an oscillation due to multiple reflections at the entrance and the exit of the constriction.[4,5] Note that, in the limit $p \to \infty$, the point-contact length approaches $L/2 \approx 2\lambda_F$, and so several peaks are expected to superpose on the plateau. The conductance at the steps decreases for larger p since the tunneling transmission through the bottleneck of the constriction becomes negligible.

In Fig. 3 we show the conductance in the presence of the short-range disorder for $p = 4$. The site energy is randomly modified with a uniform distribution of the width $\Gamma/E_F = 0.5$ The corresponding mean free path is $\Lambda/L \approx 13$. The solid lines correspond to different impurity configurations. One can see that the conductance can be both enhanced and reduced between plateaus. Howev-
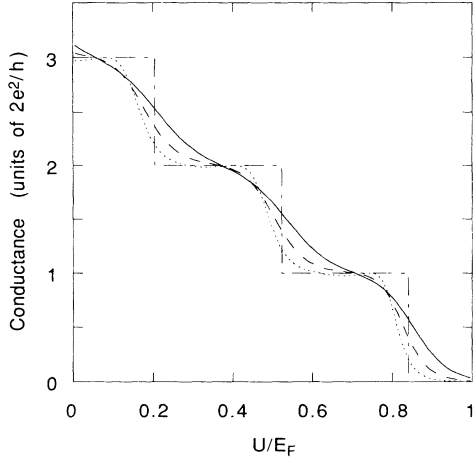
FIG. 2. The conductance of a point contact for $N_x = N_y = 32$ and $d = \lambda_F = 8.1a$. The solid, dashed, and dotted lines correspond to $p = 2$, 3, and 5, respectively. The dash-dotted line represents the number of propagating modes at the constriction. With increasing p, the effective length of the point contact is increased and the quantization becomes better.

er, it is in general suppressed below the quantized values on the plateaus.[6,9] We call attention to the fact that the conductance in the plateau region is no longer given by integer multiples of $2e^2/h$ when the short-range disorder is introduced. The upper half of Fig. 3 shows $\langle G \rangle - G_0$ and the standard deviation of the conductance $\Delta G = (\langle G^2 \rangle - \langle G \rangle^2)^{1/2}$. Here G and G_0 represent the conductance with and without presence of the disorder, respectively. The average is calculated from 25
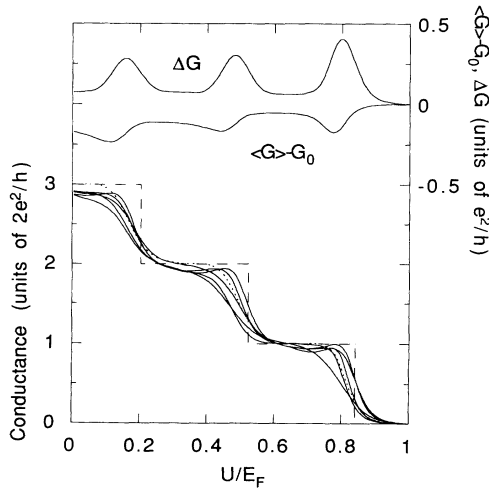

FIG. 3. The conductance of a point contact with the presence of short-range disorder for $p = 4$. The dotted line represents the conductance for a perfect sample, while different impurity configurations are assumed for the solid lines. The amplitude of the disorder is $\Gamma/E_F = 0.5$. The dashed line represents the number of propagating channels at the constriction. The conductance at plateaus is reduced below the quantized values.

equivalent samples. The amplitude of the fluctuations is maximum ($\Delta G = 0.3 \sim 0.4e^2/h$) when a new channel is barely opened and minimum ($\Delta G = 0.06 \sim 0.08e^2/h$) whenever the electron energy is near the bottom of the subband thresholds. The effects on the quantized conductance of scattering from impurities have been reported by Timp et al.[10,11] They observed time-dependent random fluctuations of the conductance with an amplitude $\Delta G \approx e^2/h$ when the Fermi energy is aligned between quantized plateaus. The time spent on each conductance value is much larger than the transit time through the constriction. Each value is thus supposed to correspond to a particular configuration of random potentials. It has been found that the fluctuations are inhibited when approaching the plateaus.[11] The numerical result shows that ΔG in the plateau region is suppressed by $\frac{1}{5}$ compared to that in the region between two plateaus. We show below that this suppression is further pronounced if one takes into account the long-range nature of the scattering potential.

The assumption of the short-range impurity potential is plausible in a metal, where scattering is almost isotropic due to good screening. Thus, the total and the transport scattering rates are identical. However, the scattering potential in GaAs has been known to be long ranged[12] due to relatively poor screening and small-angle scattering, which is less likely to affect the mobility or destroy the quantization significantly.[10] In GaAs-$Al_xGa_{1-x}As$, ionized impurities, which are the dominant source of the scattering, are separated from the 2DEG by the spacer layer. A self-consistent calculation has found that because of the long-range nature of the impurity potential the correlation length of the random potential fluctuation is large compared to the Fermi wavelength and much larger than the distance between donors.[19] In other words, the modification of the potential due to capture and emission of an electron at a single trap site corresponds to a change in U instead of a fluctuation of the lattice-site energy as used in our model.[20] Now, we adopt the following potential for an individual impurity:

$$V_{imp}(\mathbf{r}) = U_i \exp(-|\mathbf{r} - \mathbf{r}_0|/r_d) , \qquad (21)$$

where $\mathbf{r}_0$ is the position of the impurity. The decay length of the impurity potential is represented by r_d. The strength U_i is chosen randomly within the width Γ. The correction to the site energy is given as a sum of these $N_i = [LW/r_d^2]$ impurity potentials added randomly in the channel.[21] The solid lines in Fig. 4 show the conductance with the presence of the long-range impurities for several values of r_d. We expect $r_d \approx \lambda_F$, since the Thomas-Fermi screening length is typically comparable with λ_F in 2D GaAs.[12] Although the position of the plateaus is shifted in U/E_F by the long-range disorder, the conductance remains well quantized as integer multiples of $2e^2/h$. Note that we assumed a relatively large randomness, and as a result we found a considerable shift of the pinch-off energy roughly by an amount of Γ. If Γ is small compared to the energy width of the plateaus, one finds that the conductance at the center of the plateaus is almost independent of the disorder. Timp et al.[11] attributed the
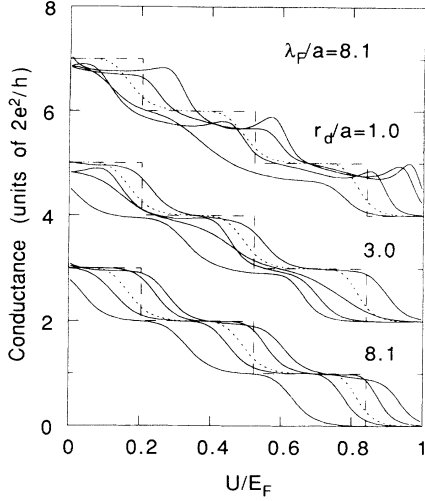
FIG. 4. The conductance of a point contact with the presence of long-range disorder for $p = 4$. The dotted line represents the conductance for a perfect sample, while different impurity configurations are assumed for the solid lines. The dashed line represents the number of propagating channels at the constriction. The amplitude of the disorder is $\Gamma/E_F = 0.5$. The range of the impurity potential r_d (the number of impurities N_i) is 1.0 (1024), 4.0 (64), and 8.1 (15) from the top to the bottom.

inhibition of the telegraph noise to the suppression of large-angle scattering in the 1D channel.[22] However, the experimental result shows the suppression of the amplitude of the fluctuations rather than an increase in the time duration on each telegraph step.[11] Our result suggests that the inhibition can be explained in terms of the long correlation length of the impurity potential. Since the conductance was quantized with 1–5 % accuracy in the experiment,[11] the correlation length of the potential fluctuation is expected to be larger than the point-contact length.[19]

The conductance quantization is well preserved as far as the correlation length of the randomness is larger than the constriction length. The effect of such long-range disorder is essentially to move the step structure in energy. The short-range potential model could overestimate the effects of the disorder. If the constriction length exceeds the correlation length, potential hills and dips appear in the channel, leading to the breakdown of the quantization. In this situation, transmission resonances through quasibound states obscure the quantization as seen in the case of $r_d/a = 1.0$ in Fig. 4. We address the effects of the randomness on the resonances in the remainder of this paper.

B. Double point contacts

The conductance of a disk structure attached to wide regions through narrow wires shows resonance structures when the Fermi energy coincides with the quasibound state energy.[23,24] We now turn to a discussion of the impurity effects on these transmission resonances. In order to calculate the conductance of the quantum dot, we as-

sume that $y_0(x)$ and $V_B(x)$ are given as follows:

$$y_0(x) = \begin{cases} \dfrac{W}{4}\left[1 + \cos\left|\dfrac{4\pi x}{L}\right|\right], & |x| > L/4 \\ 0, & |x| < L/4, \end{cases} \tag{22}$$

$$V_B(x) = \dfrac{U}{2}\left[1 - \cos\left|\dfrac{4\pi x}{L}\right|\right]. \tag{23}$$

The upper half of Fig. 5 shows $y_0(x)$ and the lower half shows the potential profile at the Fermi energy for various values of U/E_F. For these parameters, the curvatures of the potential in the x and y directions are comparable near the bottom of the quantum dot, and so one may approximate the confinement potential as $V(x,y) = m\omega^2(x^2 + y^2)/2$. In a weak-coupling limit, the quasibound-state energy is roughly given by[25]

$$E_n = \hbar\omega(n + 1), \tag{24}$$

where $n = 0, 1, 2, \ldots\ldots$. The nth energy level has $(n + 1)$-fold degeneracy.

The conductance of the quantum dot is shown in Fig. 6 as a function of U. One can see several resonance peaks with amplitude almost unity. The peak around $U/E_F = 1.5$ corresponds to the $n = 0$ bound state and the two peaks on the lowest conductance plateau correspond to the $n = 1$ bound states. The latter states are no longer degenerate due to a nonquadratic potential and a coupling to the side leads. We label these peaks A, B, and C as seen in Fig. 6, for convenience. The dashed and dotted lines show the examples of the conductance in the presence of short- and long-ranged disorder, respectively. An example of the behavior of the resonances as the strength of the disorder is increased is shown in the inset of Fig. 6 for short-range impurities. For these curves, the random
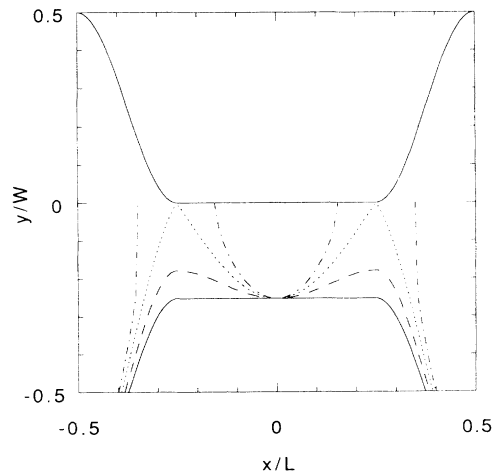

FIG. 5. A schematic illustration of a quantum dot. The upper half shows the dependence of y_0 on the position x/L. The potential profile at Fermi energy is shown in the lower half. The solid, dashed, dotted, and dash-dotted lines correspond to the barrier potential height of $U/E_F = 0$, 0.5, 1, and 1.5, respectively.
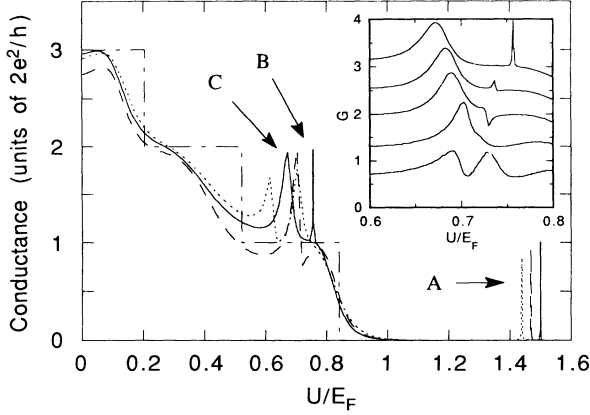
FIG. 6. The conductance of a quantum dot for $N_x = N_y = 32, d = \lambda_F = 8.1a$. The solid line shows the conductance in the absence of disorder. Short- and long-ranged potential fluctuations with amplitude $\Gamma/E_F = 0.5$ and 0.8 are assumed for the dashed and dotted lines, respectively. The number of impurities for the long-range impurity is $N_i = 15$. Inset: The effects of short-range impurities on the transmission resonances. The random site energy correction is scaled by a common factor for a particular impurity configuration. The curves from top to bottom correspond to $\Gamma/E_F = 0$, 0.2, 0.3, 0.6, and 0.8, respectively. The curves are offset by e^2/h, for clarity.

correction of each site energy is scaled by a common factor for a particular impurity configuration. With increasing disorder, the resonance peak B turns out to be a dip and then becomes a broad peak. We note that the details of the behavior of the resonance B depend on the impurity configuration, i.e., in some cases the resonance does not turn to a dip or it remains a dip. On the other hand, peak C depends only weakly on the disorder. We find that the impurity effects on these peaks are generally gentler for the long-range disorder, probably because the mode mixing is less pronounced compared to the case of the short-range disorder.

In a square-shaped quantum dot with width W_d and length L_d, the resonance energy in a weak link is given by

$$E_r = \frac{\hbar^2}{2m} \left\{ \left[\frac{n\pi}{W_d} \right]^2 + \left[\frac{m\pi}{L_d} \right]^2 \right\}, \tag{25}$$

where n and m are the quantum numbers of sinusoidal wave functions in the x and y directions, respectively. In this notation, the peaks A, B, and C correspond to the indices of $(n,m) = (1,1)$, (2,1), and (1,2), respectively.[26] In the absence of disorder the confinement potential is symmetric with respect to $y = 0$, so that the resonant state B only couples with evanescent modes in the point contacts because of parity. However, it can couple to a propagating mode in the point contacts if the disorder is introduced. If the coupling is mainly due to the evanescent

modes, electrons are resonantly transmitted, whereas they are resonantly reflected if the coupling is mainly due to the propagating modes.[23,27] Therefore, the resonance may appear as a dip in the disordered sample depending on the relative strength of the mode mixing. The resonance state C couples to both propagating and evanescent modes even if the confinement potential is symmetric, so that the peak is insensitive to the disorder.

It can be shown that the resonances in the quantum-mechanical transmission probability in small systems are of the Breit-Wigner form[28]

$$|T(E)|^2 = \frac{\Gamma_r \Gamma_l}{(E - E_r)^2 + (\Gamma_r + \Gamma_l)^2/4}, \tag{26}$$

where E is the incident energy of an electron and $\Gamma_r/\hbar (\Gamma_l/\hbar)$ is the escape rate of an electron in the quasibound states in the quantum dot to the right (left) reservoir. The suppression of the amplitude of the peak A may be ascribed to the asymmetry of the escape rate in each point contact. The asymmetry is expected to be larger for the long-range disorder compared to the short-range one.

IV. SUMMARY

We have presented numerical examples of the conductance of the quantum point contact and the quantum dot taking account of the flared geometry. The model consists of a square lattice, and the smooth potential variation and the presence of disorder are incorporated within a mode-matching technique by use of the transfer-matrix technique. The elastic scattering caused by impurities is introduced through a disordered potential. For the short-range disorder, the conductance is reduced below the quantized values at the plateaus and can be both enhanced and suppressed at the transition region between the plateaus. However, the effect of the long-range disorder is mainly to shift the conductance traces in energy, and hence the fluctuation of the conductance caused by the capture and the emission of an electron in a single trap site is suppressed at the plateaus. The transport will be more adiabatic when the disorder has a long correlation length compared to the case of the δ-function-type random potential. The second example we show is the effect of the disorder on the sharp resonances in the transmission probability of a quantum dot. The transmission resonances in the quantum dot are found to appear as both peaks and dips if the symmetry of the confinement potential is destroyed through disorder depending on the strength of the randomness.

ACKNOWLEDGMENTS

[1] T. J. Thornton, M. Pepper, H. Ahmed, D. Andrews, and G. J. Davies, Phys. Rev. Lett. **56**, 1198 (1986).

[2] B. J. van Wees, H. van Houten, C. W. J. Beenakker, J. G. Williamson, L. P. Kouwenhoven, D. van der Marel, and C. T. Foxon, Phys. Rev. Lett. **60**, 848 (1988); D. A. Wharam, T. J. Thornton, R. Newbury, M. Pepper, H. Ahmed, J. E. F. Frost, D. G. Hasko, D. C. Peacock, D. A. Ritchie, and G. A. C. Jones, J. Phys. C **21**, L209 (1988).

[3] Y. Imry, in *Directions in Condensed Matter Physics,* edited by G. Grinstein and G. Mazenko (World Scientific, Singapore, 1986); L. I. Glazman, G. B. Lesovik, D. E. Khmelnitskii, and R. I. Shekter, Pis'ma Zh. Eksp. Teor. Fiz. **48**, 218 (1988) [JETP Lett. **48**, 238 (1988)]; A. Yacoby and Y. Imry, Phys. Rev. B **41**, 5341 (1990); R. Landauer, J. Phys. Condens. Matter **1**, 8099 (1989).

[4] A. Szafer and A. D. Stone, Phys. Rev. Lett. **62**, 300 (1989).

[5] G. Kirczenow, Phys. Rev. B **39**, 10 452 (1989).

[6] D. van der Marel and E. G. Haanappel, Phys. Rev. B **39**, 7811 (1989).

[7] C. S. Chu and R. S. Sorbello, Phys. Rev. B **40**, 5941 (1989).

[8] P. F. Bagwell, Phys. Rev. B **41**, 10 354 (1990); A. M. Kriman, B. S. Haukness, and D. K. Ferry, in *Granular Nanoelectronics,* edited by D. K. Ferry, J. R. Barker, and C. Jacoboni (Plenum, New York, 1991), p. 523.

[9] T. Ando, Phys. Rev. B **44**, 8017 (1991).

[10] G. Timp, R. Behringer, S. Sampere, J. E. Cunningham, and R. E. Howard, in *Nanostructure Physics and Fabrication,* edited by M. A. Reed and W. P. Kirk (Academic, New York, 1989), p. 331.

[11] G. Timp, R. E. Behringer, and J. E. Cunningham, Phys. Rev. B **42**, 9259 (1990); G. Timp and R. E. Howard, Proc. IEEE **79**, 1188 (1991).

[12] T. Ando, A. B. Fowler, and F. Stern, Rev. Mod. Phys. **54**, 437 (1982); S. Das Sarma and F. Stern, Phys. Rev. B **32**, 8442 (1985).

[13] K. S. Rall, W. J. Skocpol, L. D. Jackel, R. E. Howard, L. A. Fetter, R. W. Epworth, and D. M. Tennant, Phys. Rev. Lett. **52**, 228 (1984); M. J. Uren, D. J. Day, and M. J. Kirton, Appl. Phys. Lett. **47**, 1195 (1985).

[14] Y. Avishai and Y. B. Band, Phys. Rev. Lett. **62**, 2527 (1989); R. L. Schult, H. W. Wyld, and D. G. Ravenhall, Phys. Rev. B **41**, 12 760 (1990).

[15] D. S. Fisher and P. A. Lee, Phys. Rev. B **23**, 6851 (1981); D. J. Thouless and S. Kirkpatrick, J. Phys. C **14**, 235 (1981).

[16] S. E. Laux, D. J. Frank, and F. Stern, Surf. Sci. **196**, 101 (1988).

[17] R. Landauer, Philos. Mag. **21**, 863 (1970).

[18] M. Büttiker, Phys. Rev. B **41**, 7906 (1990).

[19] J. A. Nixon, J. H. Davies, and H. U. Baranger, Phys. Rev. B **43**, 12 638 (1991).

[20] M. Büttiker, in *Granular Nanoelectronics,* edited by D. K. Ferry, J. R. Barker, and C. Jacoboni (Plenum, New York, 1991), p. 181.

[21] In the numerical simulation, we added $9N_i$ impurities in a $3N_x \times 3N_y$ lattice and the central $N_x \times N_y$ lattice was used as a model disorder potential.

[22] H. Sakaki, Jpn. J. Appl. Phys. **19**, L735 (1980).

[23] Y. Takagaki and D. K. Ferry, Phys. Rev. B **45**, 13 494 (1992).

[24] C. G. Smith, M. Pepper, H. Ahmed, J. E. F. Frost, D. G. Hasko, D. C. Peacock, D. A. Ritchie, and G. A. C. Jones, J. Phys. C **21**, L893 (1988); Y. Hirayama and T. Saku, Phys. Rev. B **39**, 5535 (1989); Solid State Commun. **73**, 113 (1990).

[25] C. G. Darwin, Proc. Cambridge Philos. Soc. **27**, 86 (1930); C. Cohen-Tannoudji, *Quantum Mechanics* (Hermann, Paris, 1977), Vol. 1, p. 727.

[26] Y. Takagaki and D. K. Ferry, Phys. Rev. B **45**, 8506 (1992).

[27] Y. B. Levinson, M. I. Lubin, and E. V. Sukhorukov, Phys. Rev. B **45**, 11 936 (1992).

[28] L. D. Landau and E. M. Lifshitz, *Quantum Mechanics* (Pergamon, Oxford, 1977).